One-Pot, Room-Temperature Conversion of CO_2 into Porous Metal−Organic Frameworks

Kentaro Kadota,[1] You-lee Hong,[3,6] Yusuke Nishiyama,[3,4] Easan Sivaniah,[1,5] Daniel Packwood,[5] and Satoshi Horike*[2,5,6,7]

[1]Department of Molecular Engineering, Graduate School of Engineering, and [2]Department of Synthetic Chemistry and Biological Chemistry, Graduate School of Engineering, Kyoto University, Katsura, Nishikyo-ku, Kyoto 615-8510, Japan

[3]NMR Science and Development Division, RIKEN SPring-8 Center and RIKEN-JEOL Collaboration Center, Yokohama, Kanagawa 230-0045, Japan

[4]JEOL RESONANCE Inc., Musashino, Akishima, Tokyo 196-8558, Japan

[5]Institute for Integrated Cell-Material Sciences, Institute for Advanced Study, Kyoto University, Yoshida-Honmachi, Sakyo-ku, Kyoto 606-8501, Japan

[6]AIST-Kyoto University Chemical Energy Materials Open Innovation Laboratory (ChEM-OIL), National Institute of Advanced Industrial Science and Technology (AIST), Yoshida-Honmachi, Sakyo-ku, Kyoto 606-8501, Japan

[7]Department of Materials Science and Engineering, School of Molecular Science and Engineering, Vidyasirimedhi Institute of Science and Technology, Rayong 21210, Thailand

Abstract:

We demonstrate the one-pot synthesis of highly porous crystalline metal−organic frameworks, [Zn_4O(piperazine dicarbamate)$_3$], an analogue of [Zn_4O(1,4-benzenedicarboxylate)$_3$] (MOF-5), directly from atmospheric pressure CO_2 gas and piperazine derivatives at 25 °C. The structures showed high CO_2 contents over 30 wt% and surface areas of 1270−2366 $m^2\ g^{-1}$. We also show that the synthesis is feasible even by the use of 400 ppm of CO_2.

Synthesis of functional materials using renewable resources under ambient conditions is one of the largest challenges realizing sustainable chemistry.[1,2] CO_2 is one of the most attractive renewable carbon resources, and it has many advantages such as high natural abundance, easy availability and less toxicity.[3] While showing promising characteristics as a carbon source, CO_2 has presents difficulties to synthesis due to its inherent inertness when employed in chemical reactions. To overcome its inertness, high-energy reactants, severe reaction conditions such as high pressures and temperatures, and metal complex catalysts have been developed for the conversion of CO_2 into organic polymers[4-6] and carbon nanomaterials.[7,8] The direct conversion of CO_2 into functional materials under ambient pressures and temperatures still remains a synthetic challenge.

Metal−organic frameworks (MOFs) or porous coordination polymers (PCPs) are porous materials formed by metal ions and bridging organic linkers showing a wide range of functionality such as gas storage/separation, catalysis, and ionic/electronic condution.[9-11] Whereas various synthetic protocols and crystal structures of MOFs have been reported to date,[12-14] the synthesis of MOFs using CO_2 as a direct source remains unexplored. CO_2 hardly ever works as a bridging linker by itself[15] and therefore the chemical transformation of CO_2 into a bridging linker is necessary to construct MOF structures. One representative class of linkers for MOFs are carboxylates such as terephthalate, and the well-defined coordination orientation of carboxylates have enabled the rational design of porous structures. Meanwhile, synthesis of di- or tri-carboxylates, which can work as MOF linkers, from CO_2 is limited and often requires high-energy reactants, catalysts, and/or harsh conditions in multistep reactions.[16] Carbonate (CO_3^{2-}) and formate (HCO_2^-) can be formed from CO_2 at relatively mild conditions without catalysts, but they are not suitable for the construction of highly porous structures due to the small linker sizes.[17,18]

Carbamate ($[O_2C\text{-}NR_2]^-$) is an anionic species formed through nucleophilic attack by a primary or secondary amine on CO_2.[19,20] The reactivity of various alkylamines with CO_2 and the molecular structures of the resulting carbamates have been widely studied. In the Cambridge Crystallographic Data Centre (CCDC) database, many discrete metal-carbamate complexes (ca. 400 reports) have been reported and typical coordination geometries are known, such as paddle wheel geometries ($M_2(CO_2)_4$).[20] Nevertheless, carbamate-based extended coordination structures are limited (17 compounds) in the CCDC database, and none of them displays permanent porosity (Table S1, Figure S1). This is because mono-carbamate linkers are exclusively employed, which are likely to lead to a dense structure.

To construct highly porous carbamate-based MOFs, piperazine (H_2PZ), a cyclic secondary diamine, was selected as a precursor for the carbamate linker. This is because H_2PZ reacts with two molecules of CO_2 to produce the dicarbamate salt of $[H_4PZ][PZ(CO_2)_2]$ under the mild condition of 25 °C and 0.1 MPa as shown in Figure 1A.[21,22] Piperazine-1,4-dicarbamate (PDC = $[PZ(CO_2)_2]^{2-}$) has two coordination sites located at opposite ends of a six-membered ring, which in turn defines the bridging orientation of the metal ions. No extended coordination network consisting of PDC has yet been reported. When considering the design principle of MOFs, multinuclear metal clusters, or so-called secondary building units (SBUs), are essential to construct targeted porous structures.[23,24] The octahedral $[Zn_4O(CO_2)_6]$ has afforded highly porous MOFs with either aromatic and aliphatic carboxylates, e.g. $[Zn_4O(BDC)_3]$ (MOF-5, BDC = benzene-1,4-dicarboxylate),[25] $[Zn_4O(BCPBD)]_3(BBC)_4]$ (DUT-60, H_2BCPBD = 1,4-bis-*p*-carboxyphenylbuta-1,3-diene, BBC^{3-} = 1,3,5-tris(4'-carboxy[1,1'-biphenyl]-4-yl)benzene),[24] and $[Zn_4O(CDC)_3]$ (CUB-5, CDC = cubane-1,4-dicarboxylate).[26] The mono-carbamates are reported to form the same coordination geometry to afford the discrete $[Zn_4O(NR_2CO_2)_6]$ (HNR_2 = piperazine and dimethylamine).[27] Here,

we present a one-pot synthetic method to convert atmospheric pressure of CO_2 directly into highly porous carbamate-based MOFs at 25 °C.

The synthesis of $[Zn_4O(PDC)_3]$ (**1**) was carried out in a one-pot procedure using atmospheric pressure (0.1 MPa) of CO_2 at 25 °C. Flowing CO_2 (>99.99%) into a solution of $Zn(OAc)_2{\cdot}2H_2O$ (40 mM), H_2PZ (30 mM) and 1,8-diazabicyclo[5.4.0]undec-7-ene (DBU, 120 mM) in dehydrated *N*,*N*-dimethylformamide (DMF) and 2-propanol (iPrOH) immediately lead to the formation of a white precipitate. The obtained precipitate was collected by filtration and washed with iPrOH. After drying at 80 °C under vacuum, solvent-free **1** was obtained in high (80%) yield (Figure 1B). DBU, a strong non-nucleophilic base, was employed to enhance the reactivity of H_2PZ toward CO_2 by the deprotonation of H_2PZ, whereas the synthesis of **1** is also possible without DBU (Figure S28).[19,28] A control experiment using nucleophilic NaOH instead of DBU lead to the formation of a low-crystalline phase which is different from **1** (Figure S29). This is because NaOH competes with H_2PZ during the nucleophilic reaction toward CO_2. The synthesis of **1** is also possible using $Zn(NO_3)_2{\cdot}6H_2O$ instead of $Zn(OAc)_2{\cdot}2H_2O$. The following structures analogous to **1** were synthesized using H_2PZ derivatives in substantial yield (59−84%, Figure S24−25): $[Zn_4O(S\text{-mPDC})_3]$ (**2**; *S*-mPDC = *S*-(+)-2-methylpiperazine dicarbamate), $[Zn_4O(R\text{-mPDC})_3]$ (**3**; *R*-mPDC = *R*-(−)-2-methylpiperazine dicarbamate) and $[Zn_4O(dmPDC)_3]$ (**4**; dmPDC = *trans*-2,5-dimethylpiperazine dicarbamate). Whereas the described synthetic protocols were unable to produce large crystals suitable for single-crystal X-ray diffraction, the microcrystalline powder was characterized by powder X-ray diffraction (PXRD) under Ar. The PXRD patterns of **1**−**4** resemble the simulated pattern of MOF-5, suggesting that **1**−**4** has a periodic structure similar to MOF-5 (Figure S27).

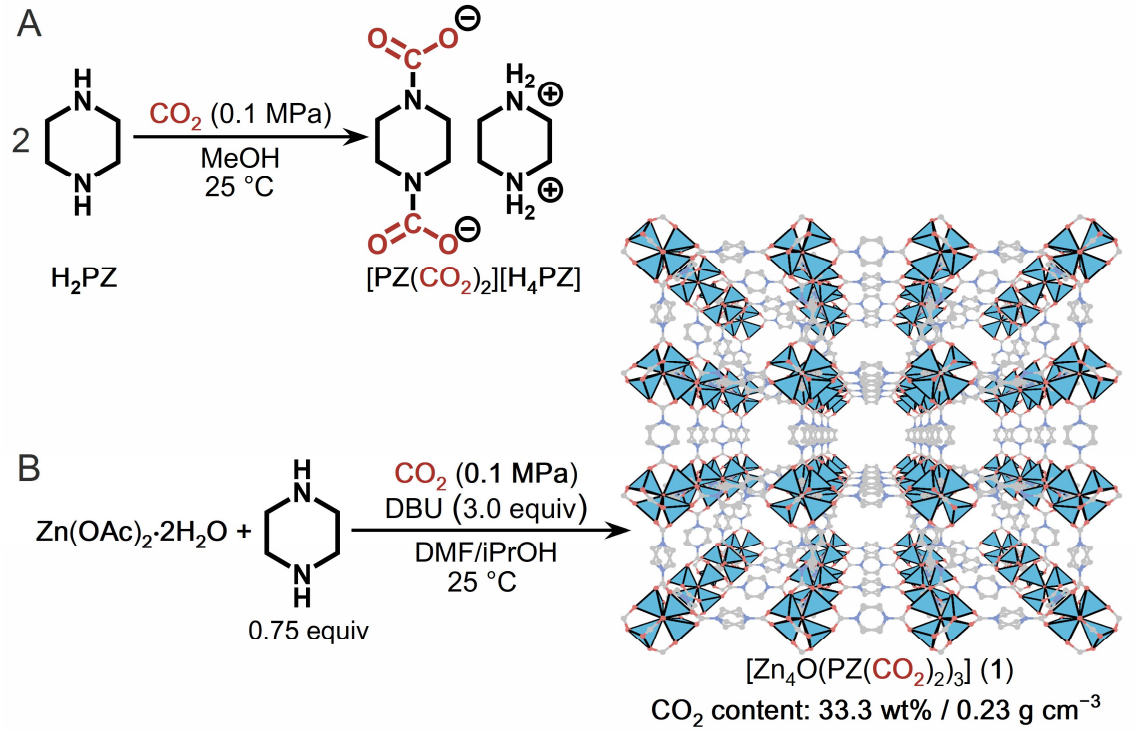

Figure 1. (A) Formation of the carbamate salt, $[H_4PZ][PZ(CO_2)_2]$ through the reaction of H_2PZ and CO_2. (B) Schematic illustration of the formation of **1** using atmospheric pressure of CO_2 at 25 °C.

To confirm the formation of PDC from H_2PZ and CO_2, solid-state nuclear magnetic resonance (SSNMR) experiments were carried out on **1** under Ar. The ^{1}H-^{13}C cross-polarization magic angle spinning (CP-MAS) SSNMR spectrum of **1** under Ar displays two peaks at 43.6 and 161.4 ppm (Figure 2A). The ^{13}C peak at 161.4 ppm is a good match with the signal of carbamate carbon ($-NCO_2^-$).[29] The ^{1}H-^{13}C heteronuclear correlation (HETCOR) NMR spectrum clearly shows the aliphatic proton of piperazine ($-CH_2-$) is correlated not only to the covalently bonded ^{13}C peak at 43.6 ppm but also to the carbamate carbon, indicating the formation of PDC.[30] To characterize the coordination geometry of Zn^{2+} in **1**, synchrotron X-ray absorption spectroscopy (XAS) at the Zn K-edge was performed on **1** under Ar. The X-ray absorption near edge structure (XANES) spectrum of **1** is qualitatively identical to that of $[Zn_4O(Me_2NCO_2)_6]$ (Figure S36). Further quantitative analysis was carried out to provide information on the first Zn coordination shell in the extended X-ray absorption fine structure (EXAFS). Figure 2B shows curve fitting on the first shell of the EXAFS spectrum of **1**. The coordination number was found to be 3.7 ± 0.2, which is reasonable for the tetrahedral Zn−4O.[31,32] Furthermore, we found that the Fourier transform infrared (FTIR) spectrum of **1** under Ar exhibits a characteristic peak at 522 cm^{-1} (Figure S37). The peak is in good agreement with the stretching vibration of μ_4-O−Zn of the $[Zn_4O(CO_2)_6]$ cluster[27], further confirming the formation of $Zn_4O(CO_2)_6$. The FT-IR spectra of **2**–**4** also exhibit peaks at 521−525 cm^{-1}, which

correspond to the stretching vibration of μ_4-O−Zn (Figure S37). The results of EXAFS and FT-IR confirm the formation of $[Zn_4O(CO_2)_6]$ in **1**−**4**.

To determine the crystal structures, synchrotron PXRD patterns were collected on **1**−**4** under Ar (λ = 0.999000 Å). The PXRD pattern of **1** was indexed in a cubic system, and Le Bail fitting was performed to extract refined unit cell parameters and to integrate the intensities. Because the solid-state NMR, XAS and FT-IR results confirmed the presence of $[Zn_4O(CO_2)_6]$ and PDC^{2-} in **1**, a plausible crystal model was obtained from the MOF-5 structure by replacing BDC^{2-} with PDC^{2-}.. Accordingly, Rietveld refinement against the experimental diffraction pattern results in a converged refinement and low *R* factors in Figure 2C (*Fm*−3*m*, *a* = 24.7739 Å, R_p = 3.07%, R_{wp} = 3.90%). The crystal structures of **2**−**4** were determined in the same manner as **1** by Rietveld refinement (Figure S8−13, 32−34) and each of **1**−**4** show cubic structures that are isostructural to MOF-5. The cell length of **1** is smaller than that of MOF-5 (*a* = 25.6690 Å) with good agreement of the length of each linker (5.5 vs. 5.7 Å).[25] Static disorder was observed in the PDC^{2-} in the structure (Figure S6−7). The full-width-half-maximum (FWHM) on the first Bragg peaks indicates that **2** has the highest crystallinity among **1**−**4** (Figure S26, 0.205, 0.0406, 0.0617, and 0.0540° for **1**−**4**, respectively).[33] Based on the crystal structures and chemical compositions, high gravimetric and volumetric contents of CO_2 in **1**−**4** were calculated as 30.1 to 33.3 wt% and 0.227 to 0.231 g cm^{-3}, respectively (Table S4, Figure S14).

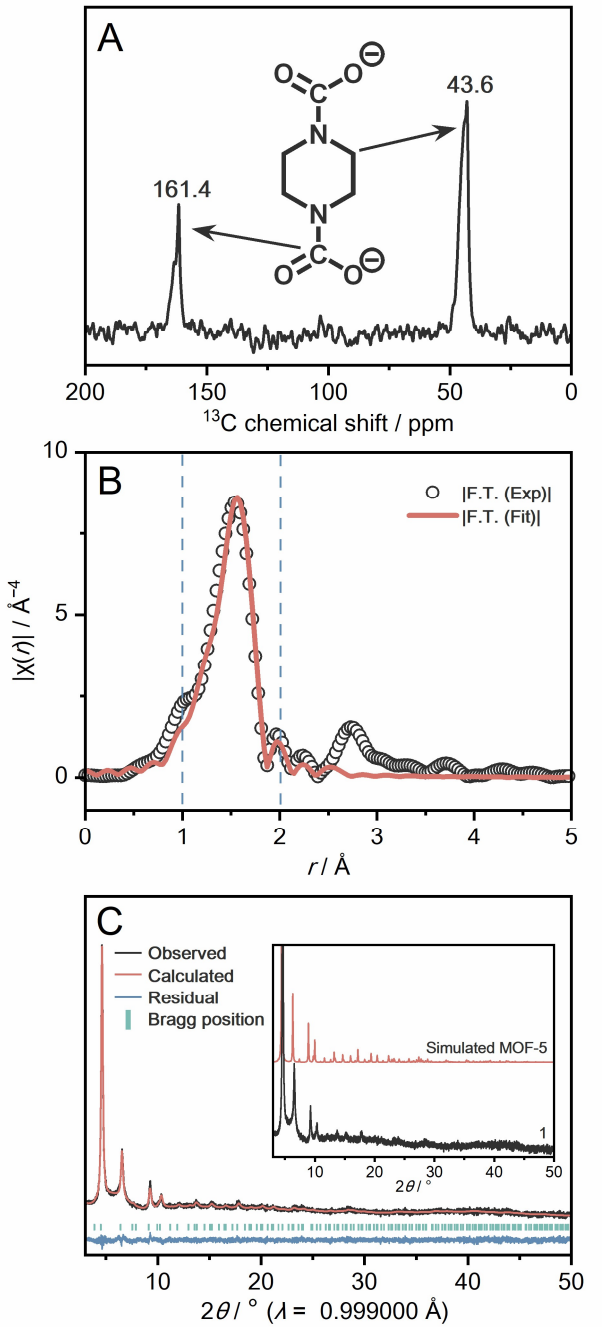

Figure 2. (A) 1D ^{13}C CP-MAS SSNMR spectrum of **1**. (B) Zn K-edge EXAFS spectrum of **1** (black circles) and fits (red solid line). The fitting range is 1.0–2.0 Å in r-space (blue dotted line). (C) Rietveld refinement of **1**. Inset: PXRD patterns of **1** (black) and the simulated MOF-5 (red).

The scalability of the described synthetic protocol was tested. **2**, showing the highest crystallinity, was synthesized on a gram scale under air using non-dehydrated DMF/iPrOH. The PXRD pattern of the **2** synthesized on the large scale under air was a good agreement with the simulated pattern of **2**, indicating that the synthetic protocol does not require severe dehydrated conditions (ca. 50 g, 83%

yield, Figure S22−23, 31). One of the synthetic challenges is to utilize atmospheric concentration of CO_2 (400 ppm in the air) for the reactions.[8,34] Dried air at 0.1 MPa containing ca. 400 ppm of CO_2 was employed for the synthesis of **1** instead of pure CO_2. Crystalline **1** was obtained using dried air, whereas the crystallinity is slightly lower than **1** synthesized from pure CO_2, due to the lower concentration of CO_2 (Figure S30).

Most carbamate ions are thermodynamically unstable because CO_2 is readily released with the dissociation of carbamate bonds upon heating or reduction of pressure.[19,28] The lability of carbamate ions should therefore impair the thermal stability of a MOF. To investigate the thermal stability of carbamate incorporated into the framework of **1**, thermal gravimetric analysis (TGA), temperature-programmed desorption (TPD), and theoretical calculations were also performed. The organic salt of the PDC^{2-}, $[H_4PZ][PZ(CO_2)_2]$ was also evaluated for comparison. The TGA profiles of each activated sample were collected under Ar and the onset temperatures for the weight loss were 90 °C (for $[H_4PZ][PZ(CO_2)_2]$), 274 °C (for **1**), 297 °C (for **2**), 289 °C (for **3)**, and 285 °C (for **4**), respectively (Figure 3A, S38). The release of CO_2 from $[H_4PZ][PZ(CO_2)_2]$ and **2**, which shows the highest thermal stability, were further characterized by TPD experiments as shown in Figure 3A. The peak maxima for released CO_2 (m/z = 44) were observed at 105 and 331 °C for $[H_4PZ][PZ(CO_2)_2]$ and **2**, respectively, which shows a good agreement with the weight loss observed by TGA. The results indicate that the formation of MOFs prevents the release of CO_2 upon heating. This is along with the previous reports of the stabilization of the thermally unstable linkers in the lattices of MOFs.[35,36] The stabilization of carbamate was further studied using density functional theory (DFT) calculations of the bond energy between Zn^{2+} and PDC^{2-} using the a hybrid exchange-correlation functional. A simplified structure model was employed for the calculations, consisting of two $[Zn_4O(CO_2)_6]$ clusters having acetates (OAc^-) as capping groups bridged by single PDC^{2-}, $[Zn_4O(OAc)_5]_2$(PDC). The total energy of the model was calculated varying the distance between Zn^{2+} and oxygen atoms of PDC^{2-} in the range of 1.51 to 4.43 Å in Figure 3B. As the Zn−O distance decreases from 4.50 Å, the potential energy decreases and reaches a minimum of −583 kJ mol^{-1} at the Zn−O distance of 1.96 Å in Figure 3C. This bond strength is only slightly weaker than the one calculated for a simplified MOF-5 model (−590 kJ mol^{-1}), as shown in Figure S39. Moreover, the two potential energy curves have a similar shape, indicating a similar Zn^{2+}-oxygen atom bonding interaction as in MOF-5. These results indicate the stabilization by coordination interaction between Zn^{2+} and PDC^{2-}.

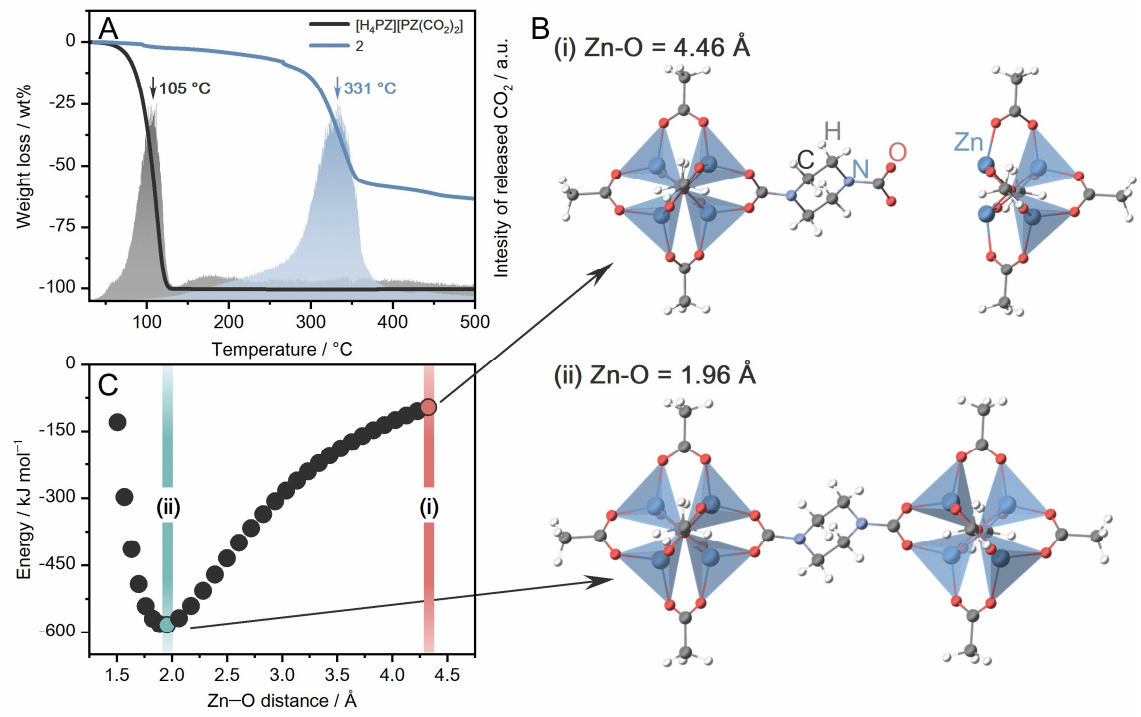

Figure 3. (A) TGA profiles of $[H_4PZ][PZ(CO_2)_2]$ (black line) and **2** (blue line) under Ar flow. CO_2-TPD profiles of $[H_4PZ][PZ(CO_2)_2]$ (black) and **2** (blue) under Ar flow. (B) Structures of $[Zn_4O(OAc)_5]_2$(PDC) calculated by the DFT using a hybrid exchange-correlation functional at the Zn−O distance of (i, top) 1.96 and (ii, bottom) 4.43 Å, respectively. (C) Potential energy curve as a function of Zn−O distance for the model structure. (i) and (ii) indicate the point of the longest Zn−O distance and the lowest potential energy, respectively.

The porosity of carbamate-based MOFs was assessed by gas adsorption experiments on the samples activated at 80 °C under vacuum. N_2 adsorption data at 77 K for **1**−**4** feature a steep increase of N_2 uptake at the low-pressure range, signifying adsorption in micropores of the framework (Figure 4). The Brunauer–Emmett–Teller (BET) surface areas for **1**−**4** were calculated as 1525, 2366, 1943, and 1270 $m^2\ g^{-1}$, respectively based on the N_2 adsorption isotherms. These values are in the middle range of the reported BET surface areas of MOF-5 (570−3800 $m^2\ g^{-1}$).[37] The PDC linkers, which are bulkier than the BDC in MOF-5, presumably lower the surface areas. **2**, which is most crystalline of **1**–**4**, shows the highest BET surface area due to its well-ordered, defect-less structure (a higher degree of crystallinity typically provides a higher surface area). The pore size distributions of **1**−**4** were calculated from the N_2 adsorption data using the non-localized density functional theory (NLDFT) model (Figure S42). All the compounds mostly contain pore sizes of ca. 1.2 nm, compared to MOF-5 at 1.4 nm. The smaller pore size of 0.7 nm is attributed to the tight corners formed between the linkers and $[Zn_4O(CO_2)_6]$ SBU.[26] The pore size distributions for **1**−**4** are broad as a

shoulder peak at 1.4 nm is observed. As observed in the crystal structures (Figure S6−13), PDC linkers display statically-disordered conformations, which might also contribute to the broad distribution of the pore sizes.

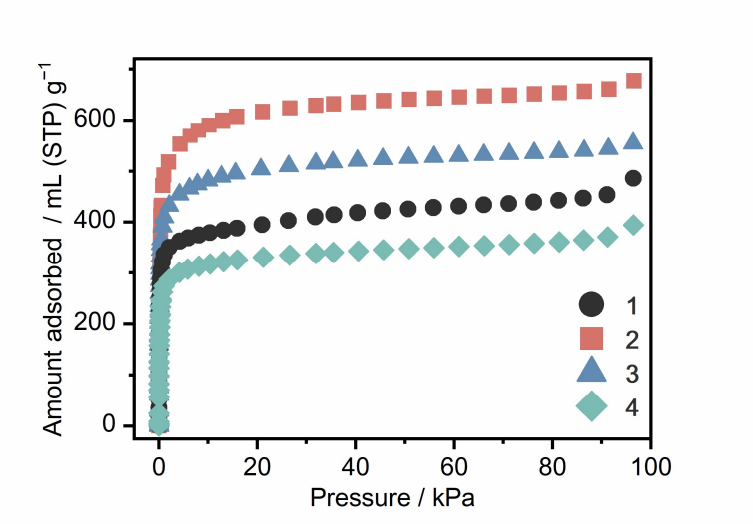

Figure 4. N_2 adsorption isotherms at 77 K for **1** (black circle), **2** (red square), **3** (blue triangle), and **4** (green rhombus), respectively.

In conclusion, we demonstrated the one-pot synthesis of crystalline carbamate-based MOF, [Zn_4O(piperazine dicarbamate)$_3$] from atmospheric pressure CO_2 and piperazine at 25 °C. Moreover, the synthetic protocol applies to a variety of piperazine derivatives. The carbamate-based MOFs show high CO_2 contents of over 30 wt% and high porosity (BET surface areas: 1270−2366 m^2 g^{-1}). The direct conversion of CO_2 into a porous MOF architecture was realized because the piperazine carbamate linkers have a coordination site orientation suitable for constructing porous structures. The piperazine carbamate linkers are stabilized by the formation of coordination bonds in the MOF structures. The approach described here therefore provides a new synthetic guideline to convert CO_2 into carbamate-based porous materials at ambient conditions.

References

1 Zhu, Y., Romain, C. & Williams, C. K. Sustainable polymers from renewable resources. *Nature* **540**, 354 (2016).

2 Marion, P. *et al.* Sustainable chemistry: how to produce better and more from less? *Green Chem.* **19**, 4973-4989 (2017).

3 Liu, Q., Wu, L., Jackstell, R. & Beller, M. Using carbon dioxide as a building block in organic synthesis. *Nat. Commun.* **6**, 5933 (2015).

4 Coates, G. W. & Moore, D. R. Discrete Metal-Based Catalysts for the Copolymerization of

CO_2 and Epoxides: Discovery, Reactivity, Optimization, and Mechanism. *Angew. Chem. Int. Ed.* **43**, 6618-6639 (2004).

5 Nakano, R., Ito, S. & Nozaki, K. Copolymerization of carbon dioxide and butadiene via a lactone intermediate. *Nat. Chem.* **6**, 325-331 (2014).

6 Grignard, B., Gennen, S., Jerome, C., Kleij, A. W. & Detrembleur, C. Advances in the use of CO_2 as a renewable feedstock for the synthesis of polymers. *Chem. Soc. Rev.* **48**, 4466-4514 (2019).

7 Chakrabarti, A. *et al.* Conversion of carbon dioxide to few-layer graphene. *J. Mater. Chem.* **21**, 9491 (2011).

8 Ren, J., Li, F.-F., Lau, J., González-Urbina, L. & Licht, S. One-Pot Synthesis of Carbon Nanofibers from CO_2. *Nano Lett.* **15**, 6142-6148 (2015).

9 Yaghi, O. M. *et al.* Reticular synthesis and the design of new materials. *Nature* **423**, 705-714 (2003).

10 Kitagawa, S., Kitaura, R. & Noro, S.-i. Functional Porous Coordination Polymers. *Angew. Chem. Int. Ed.* **43**, 2334-2375 (2004).

11 Férey, G. Hybrid porous solids: past, present, future. *Chem. Soc. Rev.* **37**, 191-214 (2008).

12 Stock, N. & Biswas, S. Synthesis of Metal-Organic Frameworks (MOFs): Routes to Various MOF Topologies, Morphologies, and Composites. *Chem. Rev.* **112**, 933-969 (2012).

13 Julien, P. A., Mottillo, C. & Friscic, T. Metal-organic frameworks meet scalable and sustainable synthesis. *Green Chem.* **19**, 2729-2747 (2017).

14 Moghadam, P. Z. *et al.* Development of a Cambridge Structural Database Subset: A Collection of Metal–Organic Frameworks for Past, Present, and Future. *Chem. Mater.* (2017).

15 Gao, G., Li, F., Xu, L., Liu, X. & Yang, Y. CO_2 Coordination by Inorganic Polyoxoanion in Water. *J. Am. Chem. Soc.* **130**, 10838-10839 (2008).

16 Tortajada, A., Ninokata, R. & Martin, R. Ni-Catalyzed Site-Selective Dicarboxylation of 1,3-Dienes with CO_2. *J. Am. Chem. Soc.* **140**, 2050-2053 (2018).

17 Kadota, K., Duong, N. T., Nishiyama, Y., Sivaniah, E. & Horike, S. Synthesis of porous coordination polymers using carbon dioxide as a direct source. *Chem. Commun.* **55**, 9283-9286 (2019).

18 Basnayake, S. A., Su, J., Zou, X. & Balkus, K. J., Jr. Carbonate-based zeolitic imidazolate framework for highly selective CO_2 capture. *Inorg. Chem.* **54**, 1816-1821 (2015).

19 Heldebrant, D. J. *et al.* Water-Lean Solvents for Post-Combustion CO_2 Capture: Fundamentals, Uncertainties, Opportunities, and Outlook. *Chem. Rev.* **117**, 9594-9624 (2017).

20 Dell'Amico, D. B., Calderazzo, F., Labella, L., Marchetti, F. & Pampaloni, G. Converting Carbon Dioxide into Carbamato Derivatives. *Chem. Rev.* **103**, 3857-3898 (2003).

21 Sim, J. *et al.* Isolation and Crystal Structure Determination of Piperazine Dicarbamate Obtained from a Direct Reaction between Piperazine and Carbon Dioxide in Methanol. *Bull. Korean Chem. Soc.* **37**, 1854-1857 (2016).

22 Conway, W. *et al.* Reactions of CO_2 with Aqueous Piperazine Solutions: Formation and Decomposition of Mono- and Dicarbamic Acids/Carbamates of Piperazine at 25.0 °C. *J. Phys. Chem. A* **117**, 806-813 (2013).

23 Tranchemontagne, D. J., Mendoza-Cortes, J. L., O'Keeffe, M. & Yaghi, O. M. Secondary building units, nets and bonding in the chemistry of metal-organic frameworks. *Chem. Soc. Rev.* **38**, 1257-1283 (2009).

24 Honicke, I. M. *et al.* Balancing Mechanical Stability and Ultrahigh Porosity in Crystalline Framework Materials. *Angew. Chem. Int. Ed.* **57**, 13780-13783 (2018).

25 Li, H., Eddaoudi, M., O'Keeffe, M. & Yaghi, O. M. Design and synthesis of an exceptionally stable and highly porous metal-organic framework. *Nature* **402**, 276-279 (1999).

26 Macreadie, L. K. *et al.* CUB-5: A Contoured Aliphatic Pore Environment in a Cubic Framework with Potential for Benzene Separation Applications. *J. Am. Chem. Soc.* **141**, 3828-3832 (2019).

27 Dell'Amico, D. B., Calderazzo, F., Labella, L., Marchetti, F. & Mazzoncini, I. *N*,*N*-dimethylcarbamato complexes of zinc. *Inorg. Chem. Acta* **359**, 3371-3374 (2006).

28 Biancalana, L., Bresciani, G., Chiappe, C., Marchetti, F. & Pampaloni, G. Synthesis and study of the stability of amidinium/guanidinium carbamates of amines and α-amino acids. *New. J. Chem.* **41**, 1798-1805 (2017).

29 Kortunov, P. V., Baugh, L. S., Siskin, M. & Calabro, D. C. In Situ Nuclear Magnetic Resonance Mechanistic Studies of Carbon Dioxide Reactions with Liquid Amines in Mixed Base Systems: The Interplay of Lewis and Brønsted Basicities. *Energy & Fuels* **29**, 5967-5989 (2015).

30 Patel, H. A. *et al.* High capacity carbon dioxide adsorption by inexpensive covalent organic polymers. *J. Mater. Chem.* **22**, 8431 (2012).

31 Hafizovic, J. *et al.* The Inconsistency in Adsorption Properties and Powder XRD Data of MOF-5 Is Rationalized by Framework Interpenetration and the Presence of Organic and Inorganic Species in the Nanocavities. *J. Am. Chem. Soc.* **129**, 3612-3620 (2007).

32 Tafipolsky, M., Amirjalayer, S. & Schmid, R. Ab initio parametrized MM3 force field for the metal-organic framework MOF-5. *J Comput Chem* **28**, 1169-1176 (2007).

33 Taddei, M. *et al.* Efficient microwave assisted synthesis of metal-organic framework UiO-66: optimization and scale up. *Dalton Trans.* **44**, 14019-14026 (2015).

34 Licht, S. *et al.* Carbon Nanotubes Produced from Ambient Carbon Dioxide for Environmentally Sustainable Lithium-Ion and Sodium-Ion Battery Anodes. *ACS Cent. Sci.* **2**, 162-168 (2016).

35 Zhang, W. *et al.* Stabilization of the Pentazolate Anion in a Zeolitic Architecture with $Na_{20}N_{60}$ and $Na_{24}N_{60}$ Nanocages. *Angew. Chem. Int. Ed.* **57**, 2592-2595 (2018).

36 Young, R. J. *et al.* Isolating reactive metal-based species in Metal–Organic Frameworks –

viable strategies and opportunities. *Chem. Sci.* **11**, 4031-4050 (2020).

37 Kaye, S. S., Dailly, A., Yaghi, O. M. & Long, J. R. Impact of Preparation and Handling on the Hydrogen Storage Properties of Zn_4O(1,4-benzenedicarboxylate)$_3$ (MOF-5). *J. Am. Chem. Soc.* **129**, 14176-14177 (2007).

38 Blum, V. *et al.* Ab initio molecular simulations with numeric atom-centered orbitals. *Comput. Phys. Commun.* **180**, 2175-2196 (2009).

39 Perdew, J. P., Burke, K. & Ernzerhof, M. Generalized Gradient Approximation Made Simple. *Phys. Rev. Lett.* **77**, 3865-3868 (1996).

40 Tkatchenko, A. & Scheffler, M. Accurate Molecular Van Der Waals Interactions from Ground-State Electron Density and Free-Atom Reference Data. *Phys. Rev. Lett.* **102**, 073005 (2009).

41 Janesko, B. G., Henderson, T. M. & Scuseria, G. E. Screened hybrid density functionals for solid-state chemistry and physics. *Phys. Chem. Chem. Phys.* **11**, 443-454 (2009).

42 Perdew, J. P. & Wang, Y. Accurate and simple analytic representation of the electron-gas correlation energy. *Phys. Rev. B* **45**, 13244-13249 (1992).

Methods

Synthesis of 1. A 100 mL of DMF solution of $Zn(OAc)_2 \cdot 2H_2O$ (878.0 mg, 4.00 mmol) was mixed with a 100 mL iPrOH solution of H_2PZ (258.4 mg, 3.00 mmol) and DBU (1.795 mL, 12.0 mmol) in a 300 mL round bottom flask at 25 °C inside an Ar-filled glovebox. The resultant transparent solution was stirred for 3 min. The flask was sealed with a rubber septum and taken outside the glovebox. CO_2 gas (>99.99%) was flowed into the round bottom flask at 25 °C. The white precipitate was formed immediately (< 10 sec). The reaction mixture was stirred under CO_2 flowing overnight to complete the reaction. The flask was purged with Ar and taken inside the glovebox. The precipitate was collected by filtration and washed with DMF and iPrOH under Ar, and dried under vacuum at 25 °C (80% yield, Calcd for $C_{18}H_{24}N_6O_{13}Zn_4$: C, 27.23; H, 3.05; N, 10.59. Found: C, 27.20; H, 4.17; N, 10.19.).

Synchrotron PXRD measurements and Rietveld refinement. Each powder sample was sealed in a Lindemann glass capillary inside an Ar-filled glove box. The synchrotron PXRD data were collected using synchrotron radiation (λ = 0.999000 Å) employing a large Debye-Scherrer camera with semiconductor detectors on the BL02B2 beamline at the Super Photon Ring (SPring-8, Hyogo, Japan). The synchrotron PXRD data of the activated samples was utilized for the analysis. The initial structures for Rietveld refinement were constructed from the reported crystal structure of MOF-5 (CCDC code: SAHYIK). All the procedures were carried out using Rigaku PDXL2 software.

SSNMR measurements. All SSNMR spectra were performed at 14.1 T on a JNM-ECZ600R

spectrometer with a 1 mm ^{1}H/X double-resonance MAS probe (JEOL RESONANCE Inc., Tokyo, Japan) under ambient temperature (~ 25 °C). 1D ^{13}C CP-MAS and 2D ^{1}H-^{13}C HETCOR SSNMR spectra were measured at MAS of 70 kHz and recycle delay of 11 sec. $\pi/2$ pulse lengths of ^{1}H and ^{13}C are 0.75 us and 1.15 us, respectively. The contact time of CP-MAS and HETCOR experiment was 4ms to observe the long range correlations between ^{1}H and ^{13}C nuclei.

XAS measurements. X-ray absorption fine structure (XAFS) measurements XAS data was collected at the BL1.1W of the Synchrotron Light Research Institute (SLRI), Thailand. The spectra at the Zn K-edge (9659 eV) were measured in a fluorescence mode using a Si(111) double-crystal monochromator. Each sample was measured in powder form by placing the sample in a plastic frame sealed under Ar with polypropylene (PP) on the side and exposed to X-rays.

Gas adsorption measurement. Gas adsorption isotherms were collected by a BELSORP-max equipped with a cryostat system. Brunauer–Emmett–Teller (BET) surface areas were calculated using N_2 adsorption isotherm data at 77 K. Each powder sample was activated at 80 °C under vacuum.

CO_2-TPD measurements. CO_2-TPD measurements were performed using a MicrotracBEL BELCAT in the temperature range of 30−500 °C at a heating rate of 10 °C min^{-1} under Ar gas flow (30 mL min^{-1}). The sample (10 mg) was packed in a quartz-based measurement apparatus under Ar atmosphere.

DFT calculations. All-electron DFT calculations were performed using the Fritz Haber Institute ab initio molecular simulations (FHI-aims) package version 171221_1.[38] Fragment structures were first relaxed using DFT with the PBE exchange-correlation functional[39] with Tkatchenko-Scheffler (TS) dispersion corrections,[40] "light" basis set settings, and no spin-polarization. Starting the relaxed structures, structures with compressed and stretched Zn---O bonds were then prepared using an in-house script. Single-point energy calculations were then performed using the HSE06 exchange-correlation functional[41] with TS dispersion corrections,[40] spin-polarization, and "tight" basis set settings. The HSE06 functional used 25 % Hartree-Fock exchange and range separation parameter 0.11 Bohr^{-1}. To explore how the choice of exchange-correlation approximation affects the results, the same calculations were also repeated using the LDA exchange correlation functional (Perdew-Wang 1992 parameterization).[42] No significant qualitative differences were observed when using the LDA functional, indicating that our conclusions should be robust to exchange-correlation approximations.

Data availability

All data generated and analyzed in this study are included in the Article and its Supplementary Information, and are also available from the authors upon request. Crystallographic information has been deposited in the Cambridge Crystallographic Data Centre under accession codes CCDC 2047156 ([H_4PZ][PZ(CO_2)$_2$]), 2047157 ([DBU][PZ(CO_2)$_2$]), 2047158 (**1**), 2047159 (**2**), 2047160 (**3**), and 2047161 (**4**).

References

38 Blum, V. *et al.* Ab initio molecular simulations with numeric atom-centered orbitals. *Comput. Phys. Commun.* **180**, 2175-2196 (2009).

39 Perdew, J. P., Burke, K. & Ernzerhof, M. Generalized Gradient Approximation Made Simple. *Phys. Rev. Lett.* **77**, 3865-3868 (1996).

40 Tkatchenko, A. & Scheffler, M. Accurate Molecular Van Der Waals Interactions from Ground-State Electron Density and Free-Atom Reference Data. *Phys. Rev. Lett.* **102**, 073005 (2009).

41 Janesko, B. G., Henderson, T. M. & Scuseria, G. E. Screened hybrid density functionals for solid-state chemistry and physics. *Phys. Chem. Chem. Phys.* **11**, 443-454 (2009).

42 Perdew, J. P. & Wang, Y. Accurate and simple analytic representation of the electron-gas correlation energy. *Phys. Rev. B* **45**, 13244-13249 (1992).

Acknowledgements

The authors thank Dr. Shogo Kawaguchi at the Super Photon Ring (SPring-8) for the synchrotron PXRD experiments. The authors thank Dr. Kanokwan Kongpatpanich at the Vidyasirimedhi Institute of Science and Technology (VISTEC) for the XAS experiments. The work was supported by the Japan Society of the Promotion of Science (JSPS) for Grant-in-Aid for Scientific Research (B) (18H02032) , Grant-in-Aid for JSPS Fellows (18J14153), and JSPS for Grant-in-Aid for Scientific Research on Innovative Areas (public offering) (19H04574).

Author contributions

K.K. and S.H. designed and planned the project. K.K. synthesized and characterized all the compounds. Y.L.H. and Y.N. carried out the SSNMR experiments. D.P. carried out the theoretical calculations. K.K. and S.H. wrote the manuscript, with the contribution from all co-authors.

Competing interests

The authors declare no conflict of interest.